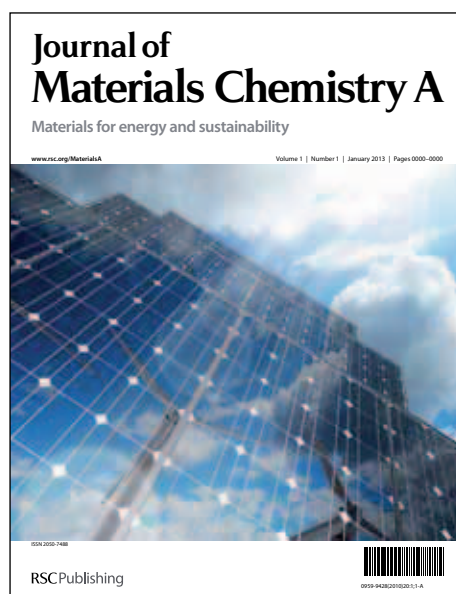


Journal of Materials Chemistry A

Accepted Manuscript



This is an *Accepted Manuscript*, which has been through the RSC Publishing peer review process and has been accepted for publication.

Accepted Manuscripts are published online shortly after acceptance, which is prior to technical editing, formatting and proof reading. This free service from RSC Publishing allows authors to make their results available to the community, in citable form, before publication of the edited article. This *Accepted Manuscript* will be replaced by the edited and formatted *Advance Article* as soon as this is available.

To cite this manuscript please use its permanent Digital Object Identifier (DOI®), which is identical for all formats of publication.

More information about *Accepted Manuscripts* can be found in the [Information for Authors](#).

Please note that technical editing may introduce minor changes to the text and/or graphics contained in the manuscript submitted by the author(s) which may alter content, and that the standard [Terms & Conditions](#) and the [ethical guidelines](#) that apply to the journal are still applicable. In no event shall the RSC be held responsible for any errors or omissions in these *Accepted Manuscript* manuscripts or any consequences arising from the use of any information contained in them.

Cite this: DOI: 10.1039/c0xx00000x

www.rsc.org/xxxxxx

ARTICLE TYPE

Graphene Aerogel Supported $\text{Fe}_5(\text{PO}_4)_4(\text{OH})_3 \cdot 2\text{H}_2\text{O}$ Microspheres as High Performance Cathode for Lithium Ion Batteries

Sheng Han,^{§a} Jinzuan Wang,^{§a} Shuang Li,^b Dongqing Wu^{*b} and Xinliang Feng^{*bc}

Received (in XXX, XXX) Xth XXXXXXXXX 20XX, Accepted Xth XXXXXXXXX 20XX

DOI: 10.1039/b000000x

Three-dimensional (3D) macroporous graphene aerogel-supported $\text{Fe}_5(\text{PO}_4)_4(\text{OH})_3 \cdot 2\text{H}_2\text{O}$ (iron(III) hydroxide phosphate dehydrate) microspheres (GA/IHPDs) has been fabricated by hydrothermal mineralization of Fe^{3+} and PO_4^{3-} ions with the presence of graphene oxide (GO). The resulting hybrids own interconnected 3D macroporous frameworks with the IHPD particles (2 μm in diameter) encapsulated in flexible graphene sheets. Using as the cathode material in lithium ion batteries (LIBs), the GA/IHPDs hybrids show excellent reversible specific capacity of 155 mAh g^{-1} after 300 cycles at a current density of 50 mA g^{-1} and maintain the specific capacities of 80 and 56 mAh g^{-1} at the ultrahigh current densities of 2000 and 5000 mA g^{-1} , respectively. To our best knowledge, such electrochemical performance of GA/IHPDs is superior to the literature reported graphene and other carbon based LiFePO_4 or FePO_4 hybrids. With a simple fabrication procedure and desirable electrochemical performance, this method offers a highly promising candidate for commercialized cathode materials of LIBs.

1. Introduction

Owing to the low manufacturing cost, high energy density and simple maintenance requirement, lithium ion batteries (LIBs) have become a ubiquitous power source for various applications such as portable electronic devices, electric and hybrid vehicles.¹⁻³ Among the three key components (cathode, anode and electrolyte) of LIBs,⁴⁻¹⁰ cathode material is usually the most expensive one in the cell. For the advance of high performance LIBs, the developments of novel cathode materials are thus extremely crucial and deserve intensive attention. In the cathodes of LIBs, carbon components can serve as the current collector and hinder the agglomeration of active components during the charge/discharge cycling, which in turn will effectively enhance the rate performance and cycling stability of the electrode materials.¹¹⁻¹⁷ Accordingly, the excellent conductivity, high surface area, good thermal and mechanical stability of graphene make it an excellent carbon support for the cathode materials in LIBs.¹⁸⁻²⁵ Especially, three-dimensional (3D) macroscopic frameworks of graphene sheets such as graphene papers, aerogels, and foams can provide continuously interconnected macroporous structures for cathode materials with a large surface area, low weight density, and high electrochemical conductivity.²⁶⁻³² Therefore, such 3D hybrids not only possess the intriguing properties of their components but also translate the intrinsic features of the individual components into macroscopic scale. Nevertheless, the research work on 3D graphene frameworks supported cathode materials for LIBs remain rarely studied.

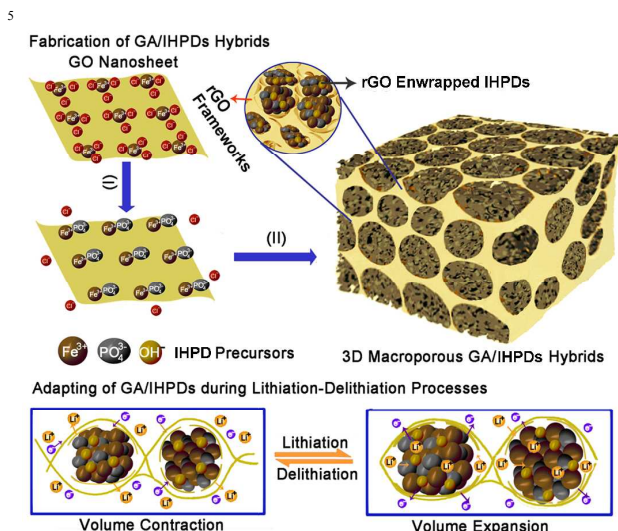
Herein, we report the facile fabrication of 3D graphene aerogel

supported $\text{Fe}_5(\text{PO}_4)_4(\text{OH})_3 \cdot 2\text{H}_2\text{O}$ microspheres (iron (III) hydroxide phosphate dehydrate, GA/IHPDs) by a one-pot hydrothermal approach. Structural characterizations indicate that the resulting hybrids own interconnected 3D macroporous frameworks with the IHPDs well encapsulated in the flexible graphene sheets. As recently reported for $\text{FePO}_4 \cdot n\text{H}_2\text{O}$,³³⁻³⁵ $\text{FeVO}_4 \cdot n\text{H}_2\text{O}$,³⁶ $\text{VOPO}_4 \cdot n\text{H}_2\text{O}$,³⁷ or $\text{MnO}_2 \cdot x\text{H}_2\text{O}$,³⁸ the presence of constitutional and/or surface water in these compounds does not inhibit their electrochemical performances vis-a-vis lithium insertion/extraction, because of the structural water nature.³⁹

As the cathode material in LIBs, the GA/IHPDs showed excellent reversible specific capacity of 155 mAh g^{-1} after 300 cycles at a current density of 50 mA g^{-1} and maintained the specific capacities of 80 and 56 mAh g^{-1} at the ultrahigh current densities of 2000 and 5000 mA g^{-1} , respectively. The electrochemical performance of GA/IHPDs hybrids is better than the reported carbon coated LiFePO_4 ,¹³ graphene based LiFePO_4 ,⁴⁰ carbon based amorphous FePO_4 ,^{2,41,42} and graphene coated amorphous FePO_4 .⁴³ The intriguing results can be attributed to the synergistic interaction between IHPDs and graphene aerogel, in which the interconnected 3D macroporous frameworks cannot only provide a continuous pathway for the transportation of Li ion and electrons but also reduce the damage caused by the periodic volume changes of the IHPDs during the charge/discharge cycles.

The overall synthetic procedure for GA/IHPDs is illustrated in Scheme 1. First, aqueous dispersion of GO was ultrasonicated with the presence of FeCl_3 to form a homogeneous suspension. Subsequently, aqueous solution of $\text{NH}_4\text{H}_2\text{PO}_4$ was slowly added. Finally the suspension was centrifuged with distilled water and

the hydrothermal treatment of the resulting brown solids led to the formation of GA/IHPDs as black sponge-like monoliths. As a controlled reaction, IHPDs were prepared in similar way, except that the GO suspension was not added.



Scheme 1 Schematic illustration of synthesis of GA/IHPDs hybrids. The fabrication process mainly includes (I) hydrolysis of metal salt on GO and (II) co-assembly and hydrothermal reduction to form GA/IHPDs hybrids. The resulting hybrids can transform from an expanded state to a contracted state during lithiation–delithiation cycles, thus enabling the stabilization of the cathode material.

2. Experimental

2.1. Preparation of GA/IHPDs hybrids

Graphene oxide (GO) was prepared from natural graphite flakes using a modified Hummers method.⁴⁴ 200 mL graphene oxide (GO, 250 mg L⁻¹) aqueous dispersion was ultrasonicated with the existence of 600 mg Iron(III) chloride (FeCl₃, Aldrich) for 30 min to form a homogeneous suspension. Subsequently, 430 mg ammonium phosphate monobasic (NH₄H₂PO₄, Aldrich) was dissolved in 50 mL of distilled water and stirred at 25 °C for 10 h. Then, the resulting brown solid products were centrifuged, washed with distilled water for three times to remove the uncombined ions in the final product. The stable suspension was sealed in a Teflon-lined autoclave and hydrothermally treated at 180 °C for 12 h. After cooling to room temperature, the as-prepared sample was freeze-dried for 35 h.

2.2. Preparation of IHPD microspheres

600 mg FeCl₃ was dissolved in 100 mL of distilled water and ultrasonicated for 30 min to form a homogeneous suspension. Subsequently, 430 mg NH₄H₂PO₄ was dissolved in 50 mL of distilled water and added slowly to the suspension solution. The following method is the same as mentioned above.

2.3. Characterization

The morphology and structure of the samples were characterized

by scanning electron microscopy (SEM, Sirion 200, 25 kV), transmission electron microscopy (TEM, JEOL JEM-2010, 200 kV), and polycrystalline X-ray diffraction (XRD, Rigaku Bruker D8 advance) with Cu K α λ = 1.5418 Å. Raman spectra was recorded on a SENTERRA with excitation from the 532 nm line of an Ar-ion laser with a power of about 5 mW. Fourier transform infrared (FTIR) was carried out on a NICOLET 6700 Fourier transform infrared spectrophotometer from 4000 to 400 cm⁻¹ by KBr sample holder method. The thermal properties of the samples were investigated using a thermogravimeter (Pyris 1, measured from room temperature to 800 °C at a heating rate of 5 °C min⁻¹ in air).

2.4. Electrochemical measurements

The obtained GA/IHPDs hybrids was mixed with carbon black (Super-p), and polyvinylidene fluoride binder with 8:1:1 weight ratio in N-methyl-2pyrrolidone solvent (Aldrich, 99.5%) until homogeneously. The slurry was dried in a vacuum oven at 60 °C for 12 h after casting onto aluminium foil with a thickness of 100 μm , and then punched into disks with diameter of 13 mm as the test electrode. The total material loading was 0.94 mg cm⁻². Pure lithium foil was used as the counter electrode. The electrolyte consisting of a solution of 1 M LiPF₆ in ethylene carbonate (EC)/dimethyl carbonate (DMC) (1:1 by volume) was obtained from Ube Industries Ltd. CR2016-type coin cell was assembled in an argon-filled glove box with the concentrations of moisture and oxygen below 1 ppm. Electrochemical test was performed using battery cyler (LAND-CT2001A) with current rates from 50 to 5000 mA g⁻¹ at voltage range of 1.5-4.5 V. Cyclic voltammetry and electrochemical impedance spectroscopy (EIS) measurements of the electrodes were carried out on an electrochemical workstation (PARSTAT 2273). The cyclic voltammograms were obtained over the potential range of 1.5-4.5 V at a scanning rate of 0.1 mV s⁻¹. The impedance spectra were recorded by applying a sine wave with amplitude of 5.0 mV over the frequency range from 100 kHz to 0.01 Hz. Fitting of the impedance spectra to the proposed equivalent circuit was performed by the code Z view.

3. Results and discussion

3.1. Structural properties

The morphologies and structure of IHPDs and GA/IHPDs hybrids were first investigated by scanning electron microscopy (SEM) and transmission electron microscopy (TEM). The pure IHPDs are sphere-like particles with average diameters of 5 μm (Fig. 1c). In contrast, GA/IHPDs had interconnected macroporous frameworks (Fig. 1a). The sizes of the macropores are in the range of submicrometer to several micrometers, and the walls of the pores consist of several layers of graphene. The partial overlapping or coalescing of flexible graphene sheets resulted in the formation of cross-linking sites of the 3D macroporous frameworks. As shown in Fig. 1b, the particles of IHPDs in the GA/IHPDs were encapsulated in the wrinkles of graphene sheets and they showed a uniform spherical morphology with average diameters of 2 μm . Compared with the pure IHPDs, the smaller size of IHPDs in GA/IHPDs hybrids can be attributed to the

restrained growth of IHPD microspheres caused by graphene. The TEM image (Fig. 1d) confirmed that IHPD particles in GA/IHPDs were wrapped by graphene sheets. Such a core-shell structure of GA/IHPDs is capable of restricting the agglomeration of IHPDs and increasing the interface contact between graphene and IHPDs, when the hybrids are used as the cathode materials in LIBs (see below).

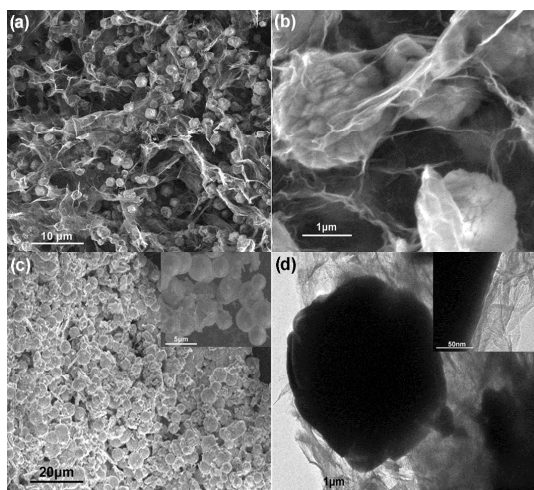


Fig. 1 Representative SEM and TEM images of GA/IHPDs hybrids: (a) overall morphology of the products; (b) high-magnification SEM images of the products; (c) pure IHPDs without reduced graphene oxide (rGO); (d) overview of an ensemble of nanoparticles at the edge of a microsphere coated with carbon.

Subsequently, powder X-ray diffraction (XRD) experiment was carried out to gain insight into the internal structure of IHPDs and GA/IHPDs. Apparently, both hybrids exhibit similar patterns (Fig. 2a), and all intensive peaks can be well indexed to rutile $\text{Fe}_5(\text{PO}_4)_4(\text{OH})_3 \cdot 2\text{H}_2\text{O}$ (JCPDS No. 45-1436),^{39,45-47} indicating that the crystallization of IHPDs during the hydrothermal treatment was not interfered by the addition of GO sheets. The structures of GO, IHPDs and GA/IHPDs were further characterized by Fourier transform infrared spectra (FTIR) and Raman spectra. In the FTIR spectrum of GO (Fig. 2b), absorption bands at 1732, 1385 and 1262 cm^{-1} can be ascribed to C=O, C=O and C-O stretching vibration, respectively. However, the intensities of these absorption decrease in the GA/IHPDs hybrids, which indicate the reduction of GO after the hydrothermal treatment.⁴⁸ IHPDs show strong absorption band at 1024 cm^{-1} , 943 cm^{-1} , 760 cm^{-1} and 605 cm^{-1} , which are associated with the stretching of Fe-O-P bond, O-P-O bond and Fe-O bond, respectively.^{2,47} And these absorption bands remain in the spectra of GA/IHPDs hybrids, confirming the successful formation of GA/IHPDs by a one-pot hydrothermal approach. In the Raman spectra of IHPDs and GA/IHPDs (Fig. 2c), peaks at 450, 577, and 1000 cm^{-1} are well matched with the vibration spectra of the PO_4^{3-} polyanion in IHPDs. On the other hand, D and G bands near 1340 and 1584 cm^{-1} are related to the bonding nature of carbon in the graphene core.

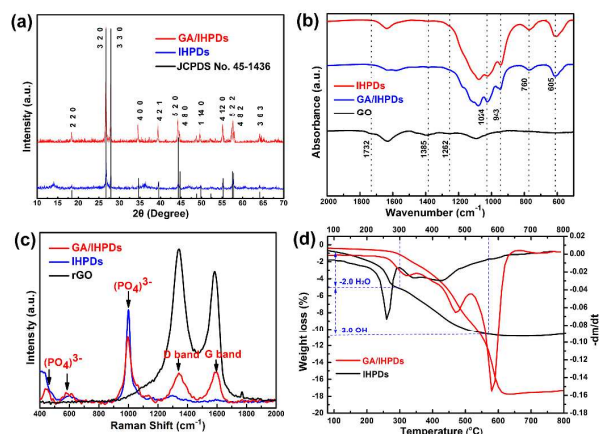


Fig. 2 (a) XRD patterns of IHPDs and GA/IHPDs; (b) FTIR spectra of IHPDs, GA/IHPDs and GO; (c) Raman spectra of IHPDs, rGO, and GA/IHPDs under an excitation laser wavelength of 532 nm; (d) TGA curves of IHPDs and GA/IHPDs.

Thermogravimetric analysis (TGA) was carried out to determine the chemical composition of the GA/IHPDs (Fig. 2d). The global analysis revealed that IHPDs loses 11% of its weight in three steps: at first between 200 and 300 °C, then between 300 and 570 °C, and finally between 570 and 650 °C. Assuming that the weight loss is associated to 2.0 H_2O and 3.0 -OH corresponds to per $\text{Fe}_5(\text{PO}_4)_4(\text{OH})_3 \cdot 2\text{H}_2\text{O}$ formula unit,³⁹ the final product contains only Fe^{3+} , O^{2-} , and PO_4^{3-} , for example as in a mixture of FePO_4 and Fe_2O_3 .⁴⁷ The decomposition temperature of GA/IHPDs hybrids is around 270 °C, indicating that graphene could improve the thermal stability of IHPDs by encapsulating them. Determined by residual content of IHPD and GA/IHPDs at 800 °C in TGA spectra, GA/IHPDs hybrid contained ~6 wt% of graphene.

3.2. Electrochemical properties

To evaluate the electrochemical reactivity of GA/IHPDs hybrids, cyclic voltammetry (CV) was investigated, as shown in Fig. 3a. The CV curves observed from GA/IHPDs clearly show redox peaks of $\text{Fe}^{2+}/\text{Fe}^{3+}$ at a scan rate of 0.1 mV s^{-1} , including a reduction peak at 2.4 V and an oxidation peak at 2.8 V, which are typical features for rechargeable batteries. The anodic peak at 2.8 V corresponds to the oxidation of Fe^{2+} to Fe^{3+} , and the reduction of Fe^{3+} to Fe^{2+} appears at 2.4 V, where the potential interval between the two redox peaks is 0.4 V.⁴⁰

The electrochemical properties of GA/IHPDs were then evaluated by galvanostatic charge/discharge cycling in a cell using lithium metal as the counter electrode at a current density of 50 mA g^{-1} (0.28C, the theoretical capacity of IHPD is 180 mAh g^{-1})^{39,49} between 4.5 and 1.5 V (Fig. 3b). The initial small plateau in the potential range of 3.2 to 2.4 V (versus Li^+/Li) associated with the Fe^{3+} to Fe^{2+} redox process for both electrodes. This is in accordance with the cathodic peak at around 2.4 V in the CV curves. The 1st cycle charge capacity was 280 mAh g^{-1} and the corresponding 1st cycle discharge capacity was 195 mAh g^{-1} , which corresponded to an irreversible capacity loss (ICL) of 30%. The 2nd cycle charge and discharge capacities were 210 and 180 mAh g^{-1} , respectively, indicating a reduced ICL of only 14%. The 2nd cycle charge curve displayed a similar shape as the first one,

suggesting that the charge-discharge process was highly reversible. In general, it is hard to achieve the theoretical capacity in a bulk or submicrometre sized particle due to its low electronic conductivity and slow Li ion diffusion rate. Facile Li ion diffusion through graphene and fast electron transport through the interconnected 3D macroporous frameworks are thus responsible for the observed high Li-storage capacity.^{2,43} It is interesting to note that the phenomenon of the increased capacity, by comparing charge curves in 100th, 200th, and 300th cycles with that in 50th cycle, is attributed to the reversible growth of a polymeric gel-like film resulting from kinetically activated electrolyte degradation.^{50, 51}

The long cycling performance of the GA/IHPDs electrode was investigated at room temperature and at a constant current density of 50 mA g⁻¹ (0.28 C), as illustrated in Fig. 3c. The capacities of the GA/IHPDs electrode in the 50th and 100th cycles were 150 and 160 mAh g⁻¹, respectively. Meanwhile, the specific capacity of the cathode after 300 cycles still maintains 155 mAh g⁻¹. The Coulombic efficiency (CE) of the GA/IHPDs electrode was above 98% when it started from the 6th cycle (Fig. S1). In contrast, in the 1st cycle, the charge capacity of the bare IHPDs electrode was about 120 mAh g⁻¹. However, the capacity continuously decreased and reached 60 and 30 mAh g⁻¹ at 300th and 900th cycles, which was only about 50% and 25% of the initial capacity, respectively, indicating poor capacity retention. The cycle performance of pure graphene electrode was poor and showed low capacity (13.4 mAh g⁻¹ at 50 mA g⁻¹).⁵² Given that GA/IHPDs hybrids only contained 6 wt% graphene, the contribution of capacity from GA in the hybrids can be negligible. The high-rate performance of the GA/IHPDs electrode was investigated to examine the possibility for the battery applications (Fig. 3d). Based on the total weight of GA/IHPDs electrode at the current rates of 50 (0.28 C), 100 (0.56 C), 500 (2.8 C), and 1000 mA g⁻¹ (5.6 C), the reversible capacities were 158, 145, 110, and 95 mAh g⁻¹, respectively. Even at ultrahigh current densities of 2000 (11.1 C) and 5000 mA g⁻¹ (27.8 C), the corresponding recharge capacities of GA/IHPDs electrode retained 80 and 56 mAh g⁻¹. The GA/IHPDs hybrids had a wonderful rate capacity, showing a reversible capacity of 165 mAh g⁻¹, which was a little higher than the first 20 cycles, demonstrating that IHPDs in a superior conducting matrix can be tolerant to high charge and discharge currents. For comparison, the capacity of IHPDs electrode dropped dramatically to only 15 and 8 mAh g⁻¹ at the current densities of 2000 (11.1 C) and 5000 mA g⁻¹ (27.8 C), respectively. To our best knowledge, such electrochemical performance of GA/IHPDs is superior to the literature reported carbon coated LiFePO₄ (79 mAh g⁻¹ at 3400 mA g⁻¹),¹³ graphene blended with LiFePO₄ (60 mAh g⁻¹ at 2550 mA g⁻¹),⁴⁰ and carbon nanotube based amorphous FePO₄ core-shell nanowires (80 mAh g⁻¹ at 1000 mA g⁻¹).²

To gain insight into the prominent electrochemical behavior of GA/IHPDs with respect to the IHPDs electrode, alternating current (AC) impedance measurements were performed before charging-discharging and after 140 charging-discharging cycles, as shown in Fig. 4a. The equivalent circuit model of the studied system is also shown in Fig. 4b to represent the internal resistance of the test battery according to literature.^{51,53} An intercept at the Z'_{re} axis at high frequency corresponds to the sum of ohmic resistance (R_s), including the ohmic resistance of the electrolyte, the electrode and the interface. The semicircle indicates the charge transfer resistance (R_{ct}), constant phase element (CPE)

represents the double layer capacitance and the SEI film capacitance, and W₁ is associated with the Warburg impedance corresponding to the lithium-diffusion process.

Before charging-discharging, it can be seen that the ohmic resistance R_s and charge-transfer resistance R_{ct} of the GA/IHPDs electrode were 4.1 and 91.3 Ω, which were a little higher than those of the IHPDs electrode (3.4 and 53.9 Ω). However, after 140 charging-discharging cycles, the R_s, 23.9 Ω and R_{ct}, 280.1 Ω of the IHPDs electrode were significantly higher than the corresponding value of 6.7 and 91.3 Ω of the GA/IHPDs electrode. It is interesting that, after 140 charging-discharging cycles, the R_{ct} of the GA/IHPDs electrode decreased. This result validates that the electrode-electrolyte interface became more compact and homogeneous during charging-discharging process, allowing the easier and faster Li ion de-intercalation/charge transfer.

3.3. Morphologies after cycles

The morphologies of the IHPDs and GA/IHPDs electrodes after 140 charging-discharging cycles were also investigated by SEM to further understand the excellent electrochemical performance of latter sample. Apparently, the IHPD spheres were broken into small piece under the impulsion of charge (Fig. S2a), which would be attributed to the poor electrochemical stability of the IHPDs electrode. In contrast, the particles of IHPDs in the GA/IHPDs electrode were still encapsulated in the flexible graphene after 140 charging-discharging cycles. The morphology of IHPDs was almost as same as that of as-prepared hybrid (Fig. S2b). Thereby, the remarkable performance of the GA/IHPDs hybrids in LIBs could be assigned to the efficient interaction between the IHPDs and graphene in the geometric confinement, where the graphene networks functioned as spacers between the individual IHPDs, thus inhibited the size and fracture formation of IHPDs. On the other hand, graphene was highly flexible, which could strain at the IHPDs surface, during periodic volume changes. Moreover, the interconnected 3D macroporous frameworks provided a continuous pathway for Li ion even at high current rates.

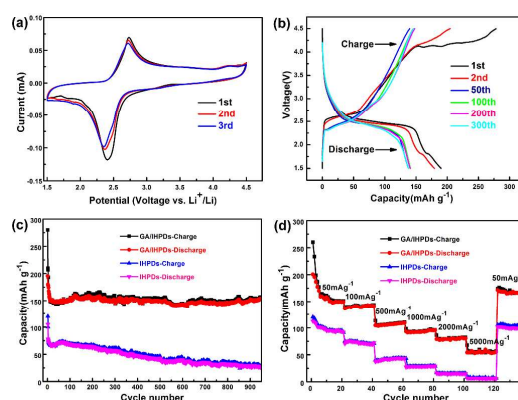


Fig. 3 Electrochemical performance of GA/IHPDs hybrids. (a) Cyclic Voltammetry (CV); (b) Discharge-charge profiles of the GA/IHPDs electrode at a current density of 50 mA g⁻¹ between 4.5 and 1.5 V: the discharge curves in the 1st, 2nd, 50th, 100th, 200th and 300th cycles; (c) Cycling performance of the GA/IHPDs and IHPDs electrodes at the current density of 50 mA g⁻¹; (d) Rate capacities of the GA/IHPDs and IHPDs electrodes between 4.5 and 1.5 V at various rates.

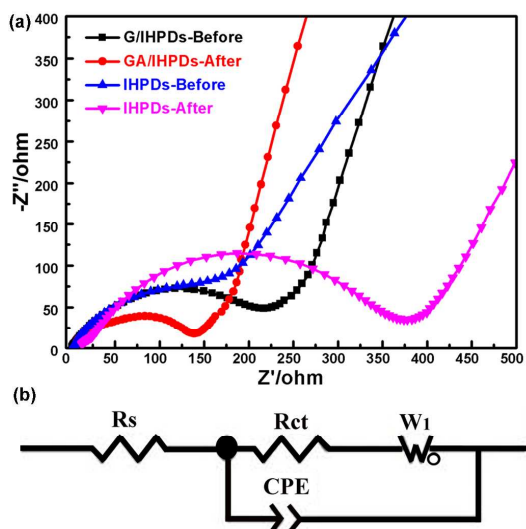


Fig. 4 (a) Nyquist plots of the GA/IHPDs and IHPDs electrodes obtained by applying a sine wave with amplitude of 5.0 mV over the frequency range from 100 kHz to 0.01 Hz; (b) equivalent circuit model of the studied system.

4. Conclusions

In summary, interconnected 3D macroporous GA/IHPDs hybrids have been prepared by a one-pot hydrothermal approach. GA/IHPDs hybrids possessed interconnected 3D macroporous frameworks with the particles of IHPDs well wrapped by graphene sheets. When they were used as the cathode materials in LIBs, such hybrids showed the enhanced rate capability and excellent cycle stability even at ultrahigh current density. This facile and environment-friendly approach may provide benefits to the scale-up synthesis of graphene-based cathode materials for LIBs in the near future.

Acknowledgements

This work was financially supported by 973 Program of China (2012CB933404 and 2013CB328804), Natural Science Foundation of China (61235007, 21102091 and 21372155), Shanghai Leading Academic Discipline Project (Project Number J51503), ShuGuang Project (Project Number 11SG54), Shanghai talent development funding (201335). We would like to thank Dr. Feng Qiu for helpful discussion about this manuscript.

Notes and references

^aSchool of Chemical and Environmental Engineering, Shanghai Institute of Technology, Shanghai 201418, China

^bSchool of Chemistry and Chemical Engineering, Shanghai Jiao Tong University, Shanghai 200240, China. E-mail: wudongqing@sjtu.edu.cn, feng@mpip-mainz.mpg.de

^cMax Planck Institute for Polymer Research, Mainz 55128, German.

^dThese two authors contributed equally to this work

† Electronic Supplementary Information (ESI) available. See DOI: 10.1039/b000000x/

1 F. Cheng, J. Liang, Z. Tao and J. Chen, *Adv. Mater.*, 2011, **23**, 1695.

- 2 S.-W. Kim, J. Ryu, C. B. Park and K. Kang, *Chem. Commun.*, 2010, **46**, 7409.
- 3 BalkeN, JesseS, A. N. Morozovska, EliseevE, D. W. Chung, KimY, AdamczykL, R. E. Garcia, DudneyN and S. V. Kalinin, *Nat. Nanotechnol.*, 2010, **5**, 749.
- 4 R. Liu, J. Duay and S. B. Lee, *Chem. Commun.*, 2011, **47**, 1384.
- 5 K. Kang, Y. S. Meng, J. Bréger, C. P. Grey and G. Ceder, in *Science*, 2006, 977.
- 6 B. Kang and G. Ceder, *Nature*, 2009, **458**, 190.
- 7 M. Armand and J. M. Tarascon, *Nature*, 2008, **451**, 652.
- 8 F. Wu, J. Chen, R. Chen, S. Wu, L. Li, S. Chen and T. Zhao, *J. Phys. Chem. C*, 2011, **115**, 6057.
- 9 A. R. Armstrong, N. Kuganathan, M. S. Islam and P. G. Bruce, *J. Am. Chem. Soc.*, 2011, **133**, 13031.
- 10 Y. Su, S. Li, D. Wu, F. Zhang, H. Liang, P. Gao, C. Cheng and X. Feng, *ACS Nano*, 2012, **6**, 8349.
- 11 Y. Wang, Y. Wang, E. Hosono, K. Wang and H. Zhou, *Angew. Chem., Int. Ed.*, 2008, **47**, 7461.
- 12 C. Sun, S. Rajasekhara, J. B. Goodenough and F. Zhou, *J. Am. Chem. Soc.*, 2011, **133**, 2132.
- 13 S. W. Oh, S.-T. Myung, S.-M. Oh, K. H. Oh, K. Amine, B. Scrosati and Y.-K. Sun, *Adv. Mater.*, 2010, **22**, 4842.
- 14 S. Yang, R. E. Bachman, X. Feng and K. Müllen, *Acc. Chem. Res.*, 2012, **46**, 116.
- 15 L. Zhi, Y.-S. Hu, B. E. Hamaoui, X. Wang, I. Lieberwirth, U. Kolb, J. Maier and K. Müllen, *Adv. Mater.*, 2008, **20**, 1727.
- 16 C. Zhang, H. B. Wu, C. Yuan, Z. Guo and X. W. Lou, *Angew. Chem., Int. Ed.*, 2012, **51**, 9592.
- 17 L. Zhang, G. Zhang, H. B. Wu, L. Yu and X. W. Lou, *Adv. Mater.*, 2013, **25**, 2589.
- 18 D. Wu, F. Zhang, H. Liang and X. Feng, *Chem. Soc. Rev.*, 2012, **41**, 6160.
- 19 M. Liang and L. Zhi, *J. Mater. Chem.*, 2009, **19**, 5871.
- 20 H. Wang, Y. Yang, Y. Liang, J. T. Robinson, Y. Li, A. Jackson, Y. Cui and H. Dai, *Nano Lett.*, 2011, **11**, 2644.
- 21 H. Wang, Y. Yang, Y. Liang, L.-F. Cui, H. Sanchez Casalongue, Y. Li, G. Hong, Y. Cui and H. Dai, *Angew. Chem.*, 2011, **123**, 7502.
- 22 G. Wang, H. Liu, J. Liu, S. Qiao, G. M. Lu, P. Munroe and H. Ahn, *Adv. Mater.*, 2010, **22**, 4944.
- 23 S. Han, D. Wu, S. Li, F. Zhang and X. Feng, *Small*, 2013, **9**, 1173.
- 24 B. Luo, S. Liu and L. Zhi, *Small*, 2012, **8**, 630.
- 25 Y. Sun, Q. Wu and G. Shi, *Energy Environ. Sci.*, 2011, **4**, 1113.
- 26 M. A. Worsley, P. J. Pauzauskie, T. Y. Olson, J. Biener, J. H. Satcher and T. F. Baumann, *J. Am. Chem. Soc.*, 2010, **132**, 14067.
- 27 M. A. Worsley, T. Y. Olson, J. R. I. Lee, T. M. Willey, M. H. Nielsen, S. K. Roberts, P. J. Pauzauskie, J. Biener, J. H. Satcher and T. F. Baumann, *J. Phy. Chem. Lett.*, 2011, **2**, 921.
- 28 B. G. Choi, M. Yang, W. H. Hong, J. W. Choi and Y. S. Huh, *ACS Nano*, 2012, **6**, 4020.
- 29 Z.-S. Wu, S. Yang, Y. Sun, K. Parvez, X. Feng and K. Müllen, *J. Am. Chem. Soc.*, 2012, **134**, 9082.
- 30 Z.-S. Wu, Y. Sun, Y.-Z. Tan, S. Yang, X. Feng and K. Müllen, *J. Am. Chem. Soc.*, 2012, **134**, 19532.
- 31 Y. Xu, K. Sheng, C. Li and G. Shi, *ACS Nano*, 2010, **4**, 4324.
- 32 S. Yang, X. Feng and K. Müllen, *Adv. Mater.*, 2011, **23**, 3575.
- 33 C. Masquelier, P. Reale, C. Wurm, M. Morcrette, L. Dupont and D.

- Larcher, *J. Electrochem. Soc.*, 2002, **149**, 1037.
- 34 Y.-S. Hong, K. S. Ryu, Y. J. Park, M. G. Kim, J. M. Lee and S. H. Chang, *J. Mater. Chem.*, 2002, **12**, 1870.
- 35 Y. Song, S. Yang, P. Y. Zavalij and M. S. Whittingham, *Mater. Res. Bull.*, 2002, **37**, 1249.
- 36 P. Poizot, E. Baudrin, S. Laruelle, L. Dupont, M. Touboul and J. M. Tarascon, *Solid State Ionics*, 2000, **138**, 31.
- 37 N. Dupré, J. Gaubicher, T. Le Mercier, G. Wallez, J. Angenault and M. Quarton, *Solid State Ionics*, 2001, **140**, 209.
- 38 S. Bach, J. P. Pereira-Ramos and N. Baffier, *Solid State Ionics*, 1995, **80**, 151.
- 39 N. Marx, L. Bourgeois, D. Carlier, A. Wattiaux, E. Suard, F. Le Cras and L. Croguennec, *Inorg. Chem.*, 2012, **51**, 3146.
- 40 J. Yang, J. Wang, Y. Tang, D. Wang, X. Li, Y. Hu, R. Li, G. Liang, T.-K. Sham and X. Sun, *Energy Environ. Sci.*, 2013, **6**, 1521.
- 41 Y. Liu, Y. Xu, X. Han, C. Pellegrinelli, Y. Zhu, H. Zhu, J. Wan, A. C. Chung, O. Vaaland, C. Wang and L. Hu, *Nano Lett.*, 2012, **12**, 5664.
- 42 J. Ryu, S.-W. Kim, K. Kang and C. B. Park, *Adv. Mater.*, 2010, **22**, 5537.
- 43 Y. Yin, Y. Hu, P. Wu, H. Zhang and C. Cai, *Chem. Commun.*, 2012, **48**, 2137.
- 44 W. S. Hummers and R. E. Offeman, *J. Am. Chem. Soc.*, 1958, **80**, 1339.
- 45 D. Li, C. Pan, R. Shi and Y. Zhu, *CrystEngComm*, 2011, **13**, 6688.
- 46 T. Roncal-Herrero, J. D. Rodríguez-Blanco, L. G. Benning and E. H. Oelkers, *Cryst. Growth Des.*, 2009, **9**, 5197.
- 47 Y. Song, P. Y. Zavalij, N. A. Chernova and M. S. Whittingham, *Chem. Mater.*, 2005, **17**, 1139.
- 48 T. Kim, H. Lee, J. Kim and K. S. Suh, *ACS Nano*, 2010, **4**, 1612.
- 49 R. Cai, H. Liu, W. Zhang, H. Tan, D. Yang, Y. Huang, H. H. Hng, T. M. Lim and Q. Yan, *Small*, 2013, **9**, 1036.
- 50 Z. Wang, D. Luan, S. Madhavi, Y. Hu and X. W. Lou, *Energy Environ. Sci.*, 2012, **5**, 5252.
- 51 D. Wang, J. Yang, X. Li, D. Geng, R. Li, M. Cai, T.-K. Sham and X. Sun, *Energy Environ. Sci.*, 2013, **6**, 2900.
- 52 S. Wang, H. Li, S. Li, F. Liu, D. Wu, X. Feng and L. Wu, *Chem. Eur. J.*, 2013, **19**, 10895.
- 53 F. Wu, G. Tan, R. Chen, L. Li, J. Xiang and Y. Zheng, *Adv. Mater.*, 2011, **23**, 5081.

40